References and Notes

1. The two most commonly noted mechanisms of crystal growth are spiral growth around a dislocation and surface nucleation followed by two-dimensional growth. Both mechanisms involve the addition of atoms to reactive surface sites from solution, vapor, or melt. W. K. Burton, N. Cabrera, F. C. Frank, *Nature* **163**, 398 (1949); L. J. Griffin, *Philos. Mag.* **41**, 196 (1950); W. K. Burton, N. Cabrera, F. C. Frank, *Philos. Trans R. Soc. London A* **243**, 299 (1951); J. Friedel, *Dislocations* (Pergamon, New York, 1964). M. F. Hochella, *Mineral-Water Interface Geochemistry*, vol. 23 of *Reviews in Mineralogy*, M. F. Hochella and A. F. White, Eds. (Mineralogical Society of America, Washington, DC, 1990), pp. 87–132.
2. R. J. Kirkpatrick, *Kinetics of Geochemical Processes*, vol. 8 of *Reviews in Mineralogy*, A. S. Lasaga and R. J. Kirkpatrick Eds. (Mineralogical Society of America, Washington, DC, 1981), pp. 321–398.
3. A. Lasaga, *Kinetics of Geochemical Processes*, vol. 8 of *Reviews in Mineralogy*, A. S. Lasaga and R. J. Kirkpatrick Eds. (Mineralogical Society of America, Washington, DC, 1981), pp. 261–320.
4. A. P. Alivisatos, *Ber. Bunsenges Phys. Chem.* **101**, 1573 (1997). One attempt to explain the absence of defects in nanocrystals is to estimate the equilibrium distance between two dislocations in the case of dislocation pileup by relating the repulsive force between two dislocations to an externally applied force (*17*). This model predicts that dislocations are unstable within crystallites of dimensions smaller than such a calculated distance. If we use published values for the shear modulus (*18*), a Burgers vector of 0.4 nm, an estimated Poisson's ratio, and hardness, the calculated minimum distance between dislocations in titania (anatase) is between 7 and 8 nm. The minimum separation is predicted to scale with the magnitude of the Burgers vector. This prediction is supported by HRTEM examination of the nanocrystalline titania used in this study, which revealed the as-synthesized particles (which are 5 to 6 nm in diameter) to be dislocation free (*19*).
5. Incorporation of impurities in a growing crystal and shear stress [in nanocrystalline aggregates (*8*)] can introduce dislocations. However, in many cases, explanations involving impurity adsorption and shear are unsatisfactory, and alternative mechanisms for dislocation formation are required.
6. R. L. Penn and J. F. Banfield, in preparation.
7. J. F. Banfield and R. J. Hamers, *Geomicrobiology: Interactions Between Microbes and Minerals*, vol. 35 of *Reviews in Mineralogy*, J. F. Banfield and K. H. Nealson, Eds. (Mineralogical Society of America, Washington, DC, 1997), pp. 86–122.
8. R. L. Penn and J. F. Banfield, *Am. Mineral.*, in press.
9. The definition of twinning was given by G. Friedel, in *étude sur les groupements cristallins*. (Bulletin de la Société de l'Industrie minérale, Quatreme série, Tomes III e IV, Societe de l'Impreimerie Theolier J. Thomas et C., Saint-Étienne, France, 1904).
10. T. Ito, *X-Ray Studies on Polymorphism* (Maruzen, Tokyo, Japan, 1950).
11. R. L. Penn and J. F. Banfield, in preparation.
12. A. A. Gribb and J. F. Banfield, *Am. Mineral.* **82**, 717 (1997).
13. R. S. Averback, H. Zhu, R. Tao, H. Höfler, *Synthesis and Processing of Nanocrystalline Powder*, D. L. Bourell, Ed. (The Minerals, Metals, Materials Society, Warrendale, PA, 1996).
14. Spiral growth about screw dislocations supplies a mechanism for generating a subset of the known polytypes [D. Pandey, A. Baronnet, P. Krishna, *Phys. Chem. Miner.* **8**, 268 (1982); R. S. Mitchell, *Z. Kristallogr.* **109**, 1 (1957)].
15. S. Amelinckx, *C. R. Acad. Sci. Paris* **237**, 1726 (1953); W. Dekeyser, *Report of the Conference on Defects in Crystalline Solids*, July 1954, H. H. Wills Physical Laboratory, University of Bristol, Bristol, UK (The Physical Society, London, 1955). V. G. Bhide, *Zs. Krist.* **109**, 81 (1957); A. Baronnet, *Prog. Crystal Growth Charact.* **1**, 151 (1978).
16. Examples include polymorphs that are long-period interstratifications of serpentine and chlorite, consisting of various proportions of layer types in regularly repeating patterns [J. F. Banfield and S. W. Bailey, *Am. Mineral.* **81**, 79 (1996)].
17. G. Nieh and J. Wadsworth, *Scr. Metall. Mater.* **25**, 955 (1991); D. Sundararaman, *Mat. Sci. Eng. B Solid* **32**, 307 (1995).
18. H. J. Hofler and R. S. Averback, *Scr. Metall. Mater.* **24**, 2401 (1990).
19. A. A. Gribb, J. F. Banfield, R. L. Penn, unpublished observations.

20. We thank M. Nespolo and T. Kogure (University of Tokyo) and H. Zhang and R. J. Hamers (University of Wisconsin–Madison) for helpful discussions. Funding was provided by NSF grant EAR-9508171, a National Physical Science Consortium Scolarship to R.L.P. (sponsored by Sandia National Laboratories), and Mineralogical Society of America Grant for Student Research in Mineralogy and Petrology to R.L.P.

28 April 1998; accepted 10 July 1998

Tetravalent Uranium in Calcite

N. C. Sturchio, M. R. Antonio, L. Soderholm, S. R. Sutton, J. C. Brannon

X-ray absorption spectroscopy and x-ray fluorescence microprobe studies of 35-million-year-old calcite from a Mississippi Valley–type zinc ore deposit indicate substitution of tetravalent uranium for divalent calcium. Thus, tetravalent uranium has a stable location in calcite deposited under reducing conditions. This result validates uranium-series dating methods (including uranium/lead dating) for ancient calcite and shows that calcite provides a sink for uranium in deep groundwater aquifers and anoxic lacustrine and marine basins.

Trace amounts of U are known to occur in calcite. This occurrence is the basis for the U-series age determinations of ancient calcites (*1*). It is used as a marine paleoenvironmental and diagenetic indicator (*2*) and may influence the transport behavior of U in groundwater aquifers (*3*). However, the location of U in the structure of calcite is problematic. Dissolved U in most natural waters generally occurs in the hexavalent oxidation state (U^{6+}) as the relatively large divalent uranyl ion (UO_2^{2+}), which is too large for regular lattice sites in calcite (*4, 5*). Uranium in the tetravalent oxidation state (U^{4+}) is generally considered to be relatively immobile because of the extremely low solubility of uranous phases (*4*). In addition, a direct structural measurement of U coordination in calcite at natural concentration levels (typically 0.1 to 10 μg/g) has been difficult to obtain.

To help elucidate the geochemical behavior of U in natural systems, we examined 35-million-year-old spar calcite having a relatively high U concentration [5 to 35 parts per million (ppm)] from a Mississippi Valley–type zinc ore deposit (*6*). We made x-ray absorption and x-ray fluorescence measurements of U in samples of this calcite and in U-rich reference materials, using synchrotron radiation (*7*).

The x-ray absorption near-edge structure (XANES) spectra of the sample and the U^{4+} reference compound have indistinguishable peak edge energies of 20,952.4 ± 0.3 and 20,952.2 ± 0.3 eV, respectively, whereas the U^{6+} reference compound has a peak edge energy of 20,954.3 ± 0.3 eV (Fig. 1). These spectra indicate that U in the sample is dominantly tetravalent.

The series of sharp peaks in the radial distribution function that is obtained by Fourier transform of extended x-ray absorption fine structure (EXAFS) spectra shows that U occupies a regular and well-defined crystallographic site in the calcite sample (Fig. 2). A multishell model (Table 1) in which U substitutes for Ca in the calcite structure corresponds with the experimental data (Fig. 2). There is one important difference between the environment of Ca in calcite and the environment of U in this calcite sample. In calcite, the first coordination shell of O about Ca forms an octahedron with a Ca-O radial distance (*R*) of 2.36 Å (*5*). The O coordination about U in the calcite sample, however, is best fit with two shells: one at 2.21 Å and one at 2.78 Å. The more distant shells, including a U-C_6 shell at 3.26 Å, a U-Ca_6 shell at 4.02 Å, and a U-Ca_6 shell at 4.98 Å, have radial distances that are indistinguishable, within error, from the corresponding shells about Ca in calcite (Table 2).

The EXAFS data are well fit with one coordination environment, ruling out the presence of multiple oxidation states or defect environments. The radial distribution function shown in Fig. 2B and the coordination shell radii listed in Table 1 are inconsistent with the occurrence of U as U^{6+} in the uranyl ion because of the absence of the characteristic strong backscattering peak from O at about 1.8 Å. Furthermore, these data are inconsistent with the occurrence of U within inclusions of uraninite (UO_2) or coffi-

N. C. Sturchio, M. R. Antonio, L. Soderholm, Argonne National Laboratory, Argonne, IL 60439, USA. S. R. Sutton, Consortium for Advanced Radiation Sources and Department of Geophysical Sciences, University of Chicago, Chicago, IL 60637, USA. J. C. Brannon, Department of Earth and Planetary Sciences, Washington University, St. Louis, MO 63130, USA.

nite ($USiO_4$) because of the absence of the strong U-O and U-U backscattering peaks that would be present at about 2.32 to 2.36 and 3.83 to 3.86 Å, respectively, in EXAFS spectra of these phases (*8, 9*).

The splitting of the first O coordination shell about U in this calcite sample is also recognized in other U-bearing minerals (Table 2). In minerals containing U^{4+}, characteristic U-O distances are 2.2 to 2.3 and 2.5 to 2.8 Å (*9–11*). In contrast, U-bearing minerals that contain U^{6+} as the uranyl ion have characteristic U-O distances of ~1.8 and 2.3 to 2.5 Å (*12*), which are not observed in our calcite sample. Two statistically indistinguishable best-fit models are consistent with our EXAFS data: one in which there are four atoms of O at 2.21 Å and two atoms of O at 2.78 Å, giving a mean U-O distance of 2.40 Å, and one in which there are three atoms of O at each distance, giving a mean U-O distance of 2.50 Å. A mean U-O distance of 2.40 Å agrees with the size of the Ca^{2+} site in calcite, where the Ca-O distance is 2.36 Å. The mean U-O distance in each best-fit model is consistent with the range of known mean U-O distances in other uranous phases (2.36 to 2.49 Å) but is substantially greater than this range in uranyl-bearing phases (2.1 to 2.3 Å) (Table 2).

The ionic radius of U^{4+} in octahedral coordination is 0.89 Å (*13*). Divalent ions such as Zn^{2+}, Mn^{2+}, and Cd^{2+} have ionic radii that range from 0.74 to 0.97 Å and can be accommodated readily in the calcite structure (*5, 14*). The principal crystal-chemical difficulty with the substitution of U^{4+} in calcite is achieving a local charge balance in the calcite lattice. A tetravalent ion in the Ca^{2+} site is undercoordinated. A coupled substitution (for example, $3Ca^{2+} \rightarrow U^{4+} + 2Na^{+}$) may be involved. Such substitutions are not inconsistent with our EXAFS data, but these data do not allow us to identify the exact substitution mechanism.

Sodium is a common impurity in calcite and may be incorporated at defect sites to maintain the charge balance in the substitution $Ca^{2+} \rightarrow 2Na^{+}$ (*15*). The range in concentration of Na required to account for the substitution mechanism proposed above is 1 to 7 ppm, on the basis of the range of measured U concentration in the calcite sample. Measuring such low Na concentrations is not possible using conventional microprobe techniques (including electron, ion, and synchrotron x-ray fluorescence microprobes). The calcite precipitated from a brine, so it may have a high Na concentration in addition to the well-documented, highly saline fluid inclusions (*16*); these features could mask the small variation in Na concentration that might correlate with U concentration.

Calcite from the locality where our sample was taken has aqueous fluid inclusions with homogenization temperatures ranging from 60° to 100°C and salinities ranging from 7 to 22 weight % (NaCl equivalent) and has rare inclusions of liquid hydrocarbon and bitumen (*16*). The presence of sulfide minerals and hydrocarbon inclusions indicates a reducing environment, consistent with the presence of U^{4+} in the calcite sample. Comparison of the U/Ca molar ratios in reducing, saline groundwaters and brines (for example, $10^{-8.0}$ to $10^{-6.4}$) (*17*) with that of our calcite sample ($\sim 10^{-5}$) indicates that U^{4+} is preferentially incorporated into calcite in such environments. In contrast, U^{6+} as the uranyl ion is generally excluded from calcite (*2, 18*).

The mapped U concentration in a portion of the calcite sample varies from about 5 to 35 ppm and is fairly uniform at the 100-μm scale (Fig. 3). Assuming that this calcite precipitated from a fluid in which U concentra-

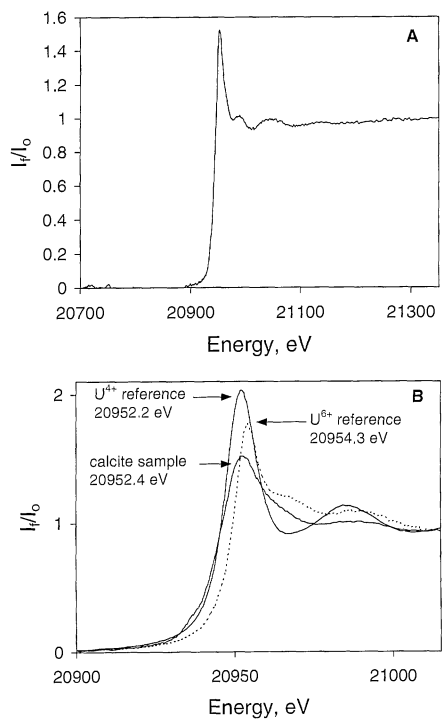

Fig. 1. (**A**) Normalized U L_2-edge EXAFS spectrum for the calcite sample, measured in fluorescence mode. (**B**) XANES portion of this spectrum, along with XANES spectra for well-characterized reference compounds of U^{4+} $[(U^{4+}P_5W_{30}O_{110})^{11-}]$ and U^{6+} $[(U^{6+}O_2)^{2+}]$ in 1 M $HClO_4$ media. The calcite XANES spectrum (lower solid line) has an edge energy indistinguishable from that of the U^{4+} reference (upper solid line), which is 2 eV lower than that of the U^{6+} reference (dashed line), indicating that U in the sample is dominantly tetravalent.

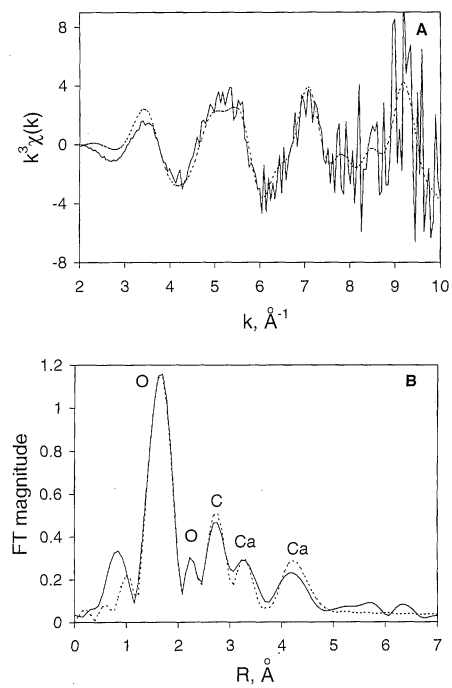

Fig. 2. (**A**) The $\mathbf{k}^3$-weighted U L_2-edge EXAFS data, $\chi(k)$, for the calcite sample (solid line) and the best-fit multishell model (dashed line) as a function of wave vector **k** in reciprocal angstroms. The data were fit from 2 to 10 $Å^{-1}$, with parameters described in Table 1. (**B**) Fourier transform (FT) of the EXAFS data (solid line), yielding a radial distribution function in angstroms from the absorber atom (uncorrected for phase shift). Strong peaks in the FT are labeled for the corresponding atomic shells used in the multishell model (dashed line). These data are consistent with substitution of U^{4+} for Ca^{2+} in the calcite sample.

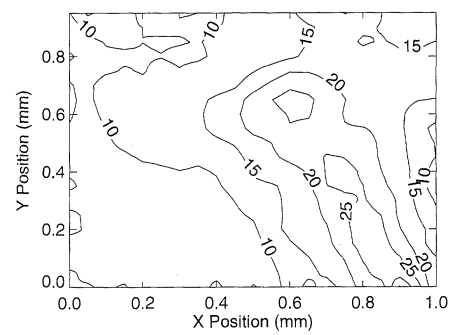

Fig. 3. X-ray fluorescence microprobe map of U in a 1-mm-by-1-mm area of the calcite sample, showing contours of U concentration in parts per million. This distribution is consistent with the substitution of U in the calcite structure and is inconsistent with inclusions of distinct U-rich compounds.

Table 1. Multishell best-fit parameters for U EXAFS of calcite sample. *N*, coordination number; *R*, radial distance; σ^2, Debye-Waller factor.

Shell	*N*	*R* (Å)	σ^2 (Å^2)
U-O	3.4 ± 0.8	2.21 ± 0.02	0.0004 ± 0.0021
U-O	2.8 ± 0.9	2.78 ± 0.03	0.0004*
U-C	6†	3.26 ± 0.06	0.006 ± 0.004
U-Ca	6†	4.02 ± 0.09	0.022 ± 0.010
U-Ca	6†	4.98 ± 0.06	0.005 ± 0.003

*Parameter fixed equal to the best-fit value for the first U-O shell. †Parameter fixed during refinement to reduce the number of fit parameters.

Table 2. Structural data for calcite and some U-bearing compounds. M, metal.

Compound	Shell	*N*	*R* (Å)	Mean *R* of M-O (Å)
Calcite (*5*)	Ca-O	6	2.36	2.36
	Ca-C	6	3.21	
	Ca-Ca	6	4.04	
	Ca-Ca	6	4.99	
Brannerite (UTi_2O_6) (*10*)	U-O	6	2.28	2.42
	U-O	2	2.82	
Calciobetafite	U-O	2	2.23	2.49
[$Ca_2(Nb,Ti)_2(O,OH)_7$] (*11*)	U-O	6	2.58	
Coffinite ($USiO_4$) (*9*)	U-O	4	2.32	2.42
	U-O	4	2.51	
	U-U	4	3.83	
Uraninite (UO_2) (*8*)	U-O	8	2.36	2.36
	U-U	12	3.85	
Uranyl compounds (*12*)	U-O	2	~1.8	2.1–2.3*
	U-O	4–6	2.3–2.5	

*Dependent on grouping.

tion was limited by uraninite solubility [$\sim 10^{-9.47}$ m at pH = 4 to 10, temperature 100 to 300°C (*19*)], we estimate that the distribution ratio $U^{4+}{}_{calcite}/U^{4+}{}_{fluid}$ had a range of about 60 to 430 ml/g. There is no evidence that U is segregated into separate U-bearing mineral inclusions (for example, uraninite grains) at this scale, in a manner analogous to the partial segregation of Sr into strontianite within aragonite coral skeletons (*20*).

The sequestration of U^{4+} in the calcite structure explains the anomalously high concentrations of U observed in calcite from reducing environments (*21*) and thus provides insight into the geochemical cycle of U in deep groundwater aquifers and anoxic lacustrine and marine basins. The incorporation of U into calcite as U^{4+} gives a potentially stable host for dispersed U over geological time scales.

References and Notes

1. K. R. Ludwig *et al.*, *Science* **258**, 284 (1992); J. C. Brannon *et al.*, *ibid.* **271**, 491 (1996).
2. A. D. Russell, S. Emerson, B. K. Nelson, J. Erez, D. W. Lea, *Geochim. Cosmochim. Acta* **58**, 671 (1994).
3. P. Zeh, K. R. Czerwinski, J. I. Kim. *Radiochim. Acta* **76**, 37 (1996).
4. D. Langmuir, *Geochim. Cosmochim. Acta* **42**, 547 (1978).
5. R. J. Reeder, in *Carbonates: Mineralogy and Chemistry*, vol. 23 of *Reviews in Mineralogy*, R. J. Reeder, Ed. (Mineralogical Society of America, Washington, DC, 1983), pp. 1–47.
6. J. C. Brannon, F. A. Podosek, S. C. Cole, in *Soc. Econ. Geol. Spec. Publ. 4* (1996), pp. 536–545.
7. X-ray absorption measurements were made using wiggler beamline 4-3 at the Stanford Synchrotron Radiation Laboratory (SSRL). The energy of the incident beam (1 by 10 mm) was selected by a Si (220) monochromator, detuned to ~50% intensity for harmonic rejection. Measurements were made in fluorescence mode at the U L_2 edge (20,948 eV); interference from Sr K-edge fluorescence precluded U fluorescence measurements at the U L_3 edge. The powdered sample (~0.5 g) was held with Kapton tape in a slotted Al plate. This plate was held at 10 K in a continuous-flow liquid He cryostat for the 20-hour duration (25 scans) of the measurements. The U $L_{\beta 1}$ fluorescence at 17,220 eV was monitored continuously with a 13-element Ge detector. X-ray absorption data were analyzed with the EXAFSPAK code (*22*). Curve fitting was performed with single-scattering theoretical phase and amplitude functions obtained from the program FEFF 6.01a (*23*). X-ray fluorescence mapping of U was done with white, bending-magnet radiation at beamline X26A at the National Synchrotron Light Source (*24*). A 1-mm^2 area of calcite was examined with a 10-μm by 10-μm beam spot size. A 50-μm^2 grid spacing was used to approximately match the U fluorescence sampling depth, with 30 s of data acquisition per pixel. The U concentration reference was National Institute of Standards and Technology standard reference material 612 (37 ppm of U in a glass matrix).
8. B. Wasserstein, *Nature* **174**, 1004 (1954).
9. L. H. Fuchs and E. Gebert, *Am. Mineral.* **43**, 243 (1958).
10. J. T. Szymanski and J. D. Scott, *Can. Mineral.* **20**, 272 (1982).
11. F. Mazzi and R. Munno, *Am. Mineral.* **68**, 2262 (1983).
12. P. C. Burns, M. L. Miller, R. C. Ewing, *Can. Mineral.* **34**, 845 (1996); H. A. Thompson, G. E. Brown Jr., G. A. Parks, *Am. Mineral.* **82**, 483 (1997).
13. R. Shannon, *Acta Crystallogr.* **32**, 751 (1976).
14. G. M. Lamble, R. J. Reeder, P. A. Northrup, *J. Phys. IV* **7**, C2793 (1997).
15. M. Ishikawa and M. Ichikuni, *Chem. Geol.* **42**, 137 (1984); E. Busenberg and L. N. Plummer, *Geochim. Cosmochim. Acta* **49**, 713 (1985).
16. J. F. Gratz and K. C. Misra, *Econ. Geol.* **82**, 1790 (1987); K. C. Misra and C. Lu, *Eur. J. Mineral.* **4**, 977 (1992).
17. J. L. Banner, G. J. Wasserburg, J. H. Chen, C. H. Moore, *Earth Planet. Sci. Lett.* **101**, 296 (1990): J. G. Zukin, D. E. Hammond, T. L. Ku, W. A. Elders, *Geochim. Cosmochim. Acta* **51**, 2719 (1987).
18. D. E. Meece and J. K. Benninger, *Geochim. Cosmochim. Acta* **57**, 1447 (1993).
19. G. A. Park and D. C. Pohl, *ibid.* **52**, 863 (1988).
20. R. B. Greegor, N. E. Pingitore Jr., F. W. Lytle, *Science* **275**, 1452 (1997).
21. C. Israelson, A. N. Halliday, B. Buchardt, *Earth Planet. Sci. Lett.* **141**, 153 (1996).
22. G. N. George and I. J. Pickering, *EXAFSPAK: A Suite of Computer Programs for Analysis of X-ray Absorption Spectra* (SSRL, Stanford, CA, 1995).
23. J. J. Rehr, J. Mustre de Leon, S. I. Zabinsky, R. C. Alberts, *J. Am. Chem. Soc.* **113**, 5135 (1991); J. Mustre de Leon, J. J. Rehr, S. I. Zabinsky, R. C. Albers, *Phys. Rev. B* **44**, 4146 (1991).
24. S. R. Sutton, M. L. Rivers, S. Bajt, K. W. Jones, *Nucl. Instrum. Methods Phys. Res. Sect. B* **75**, 5533 (1993); J. V. Smith and M. L. Rivers, in *Microprobe Techniques in the Earth Sciences*, P. J. Potts, J. F. W. Bowles, S. J. B. Reed, M. R. Cave, Eds. (Chapman & Hall, London, 1995), pp. 163–233.

25. This work was supported by the Geosciences and Chemical Sciences subprograms of the Office of Basic Energy Sciences, U.S. Department of Energy. We thank P. de Cecco (SSRL) for assistance with EXAFS measurements.

9 March 1998; accepted 4 June 1998

Coaxial Nanocable: Silicon Carbide and Silicon Oxide Sheathed with Boron Nitride and Carbon

Y. Zhang,* K. Suenaga, C. Colliex, S. Iijima

Multielement nanotubes comprising multiple phases, with diameters of a few tens of nanometers and lengths up to 50 micrometers, were successfully synthesized by means of reactive laser ablation. The experimentally determined structure consists of a β-phase silicon carbide core, an amorphous silicon oxide intermediate layer, and graphitic outer shells made of boron nitride and carbon layers separated in the radial direction. The structure resembles a coaxial nanocable with a semiconductor-insulator-metal (or semiconductor-insulator-semiconductor) geometry and suggests applications in nanoscale electronic devices that take advantage of this self-organization mechanism for multielement nanotube formation.

The discovery of pure carbon nanotubes (*1*) has resulted in extensive investigations to realize heteroatomic nanotubes; BN nanotubes (*2*) and the nanotubes in the B-C-N ternary system (*3–5*) have been reported so far. The electronic structure of such an individual tube can be controlled by its chemistry (*6*), whereas that of a pure carbon nanotube is controlled by the chirality and diameter (*7*). By combining the different types of nanotubes in axial or radial direction, nanoscaled electronic devices with a variety of functions may be realized (*4, 5, 8*). Progress has also been made in fabricating solid nanowires by